MIMO Radar and Ground-Based SAR Imaging Systems: Equivalent Approaches for Remote Sensing

Dario Tarchi, Franco Oliveri, and Pier Francesco Sammartino

***Abstract*—Currently there is an increasing interest in multiple-input multiple-output (MIMO) radars, because MIMO technology is able to provide a level of performance similar to that of a conventional antenna array, while also providing hardware and cost-related benefits. In this paper, we describe an upgrade of an existing ground-based synthetic aperture radar system (which is used for landslide monitoring) to a low-cost MIMO system. We also describe the associated low-cost/high-performance remote sensing benefits that this new configuration provides and present the results gathered by the new system. We conclude by outlining two configurations of the MIMO system with particular emphasis on antenna positioning, which has a key role in the overall performance.**

***Index Terms*—MIMO antenna positions, MIMO radars, multiple-input multiple-output (MIMO), remote sensing, synthetic aperture radar (SAR).**

I. Introduction

INNOVATIVE radar solutions are creating a revamped strategic interest and the consequent research and development in the field of security and safety. For this reason, a number of emerging problems require robust solutions which are often based on multiple sensors, including radars, as they work in a number of atmospherical conditions where other devices fail. However, historically, these sensors have been extensively used for military purposes with civilian applications being fairly limited. In this context, it is worthwhile to explore new applications, paying attention to innovative and cost-effective concepts, technologies, and solutions.

Synthetic aperture radar (SAR) imaging [1], [2] is a mature technology synthesizing an aperture bigger than the real one by exploiting the movement of the platform on which the antenna is mounted. This is one of the most advanced techniques used to generate high-resolution images even when optical systems cannot perform the task in a satisfactory manner. In the last 40 years, a number of techniques have been developed for SAR systems, including interferometry and polarimetry [3], [4], Inverse SAR, spotlight, and Doppler beam-sharpening [5]. In recent times, the idea of a low-cost frequency-modulated continuous wave (FMCW) SAR system has been developed and implemented [6]. This suggests that, with the development of low-cost electronics, it is actually possible to build at much lower costs systems that, until recently, have been quite expensive and consequently 1) to broaden the applications of conventional systems and/or 2) to find new solutions to existing problems.

The Joint Research Centre (JRC) has been active in the radar remote sensing field for approximately 20 years [7], [8]. In particular, LInear SAr (LISA), the JRC SAR system, has been used for monitoring avalanches and landslides [9], [10], employing radar interferometric techniques. With the development of the multiple-input multiple-output (MIMO) technique, it has been decided to upgrade LISA to a MIMO system.

Research on MIMO radars led to the development of two techniques based on this concept: the first one is the waveform-diversity MIMO (WD-MIMO) radar. This technique has shown that it is possible to synthesize an arbitrary antenna array starting from opportunely spaced single elements by transmitting different waveforms at the same time [11], [12]. In such a case, the spacing between the antennas is relatively narrow, i.e., comparable to the wavelength. This technique differs from the space-diversity MIMO (SD-MIMO) radar system which exploits angular diversity to acquire independent measurements of the radar cross section and increase the performance of the overall system in a number of ways and under different points of view [13]. In the latter configuration, the MIMO radar system is basically the same as a radar network where the transmitters and the receivers, which can be colocated in pairs or not, are generally widely separated from one another. The SD-MIMO is not taken into account in this paper, and for simplicity MIMO is used to indicate the WD-MIMO technique.

The MIMO SAR concept has been described in recent publications, e.g., [14]–[16]. Notwithstanding the issues in code-design [17], [18], which arise, for instance, when high Doppler shifts are expected, the application of the MIMO technique to SAR systems could be convenient under different points of view because it allows to 1) reduce dramatically the quantity of collected data, 2) have a more efficient distribution of the available power, and 3) simplify the transmission part of the system. As known, the tradeoff has to be found in the reduced control on the beam in transmission and a more complex processing of the data.

However, in this paper, a different approach is pursued: the main idea is that, when the synthetic aperture is relatively short, a ground-based synthetic aperture radar (GB-SAR) system can be replaced by a MIMO system with appropriately located antennas. In the following sections, we describe and discuss the purpose, reasons, advantages, and concept of upgrading from

Manuscript received April 7, 2010; revised January 20, 2011, June 29, 2011, and January 13, 2012; accepted March 24, 2012. Date of publication July 6, 2012; date of current version December 19, 2012.

The authors are with the Institute for the Protection and Security of the Citizen, Joint Research Centre, European Commission, 21020 Ispra, Italy (e-mail: dario.tarchi@jrc.ec.europa.eu; franco.oliveri@jrc.ec.europa.eu; pier-francesco.sammartino@jrc.ec.europa.eu).

Color versions of one or more of the figures in this paper are available online at http://ieeexplore.ieee.org.

Digital Object Identifier 10.1109/TGRS.2012.2199120

Fig. 1. LISA's antennas on the rail.

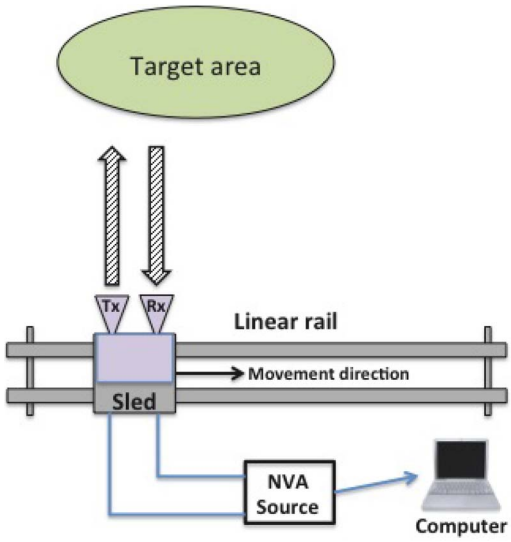

Fig. 2. Scheme of LISA system architecture.

SAR to MIMO, and we provide the first results of a short-range MIMO system, showing real data from the new upgraded system. In particular, Section II describes briefly the old system and the reasons to improve it through the MIMO technique, which is summarized in Section III. Section IV describes the new system, and Section V provides the results along with some of the gathered data. Finally, in Sections VI and VII, we discuss the main achievements of this paper, and we provide an insight on further developments.

II. Background: LISA, the JRC SAR System

This section gives a short description of the LISA system and explains in detail the reasons for replacing the SAR aperture with the MIMO aperture.

The JRC achieved significant results with the design, implementation, and licensing of LISA (Fig. 1) for ground displacement (landslide) monitoring [9], [10], [19]. Fig. 2 shows the core of LISA, which is a stepped frequency (SF) GB-SAR. The transmitter and the receiver are mounted beside one another in a quasimonostatic configuration on a mechanical linear rail, which is computer controlled, synthesizing a linear aperture along the azimuth direction. The high-frequency front-end is based on a coherent up and down frequency conversion and can perform measurements in the C and Ku bands [19]. The signal is generated by a SF CW procedure based on a vector network analyzer (VNA). The entire system is controlled by a computer, which also stores the acquired data. The processing includes a coherent SAR algorithm and interferometric techniques. LISA's acquisition time is not faster than a few minutes, but that is not a problem, as all the targeted (geological) phenomena can be observed within this time scale. Nevertheless, this system is not suitable for detecting moving targets. The data processing time does not represent a crucial parameter, as it is at least an order of magnitude faster than the acquisition time. Currently, LISA is still the most advanced tool for landslide monitoring, and its application to avalanche monitoring is being started. The most significant specifications and performance of LISA are summarized in Table II, together with the parameters of the new system [Mimo-Enhanced LInear Short SAr (MELISSA)].

Notwithstanding the good performance of LISA [20], it suffers a few drawbacks which can be summarized as follows:

i) Size: the synthetic aperture is limited by the rail length. As a consequence, the resolution is not as good as that of space and airborne SAR systems, where the aperture is not limited (at least in theory). As well, the HW occupies a large volume that goes beyond the linear dimensions of the system.
ii) Precision and cost: since the antennas have to be placed precisely along the rail, the rail itself and the controller have to be extremely accurate. This impacts directly on the price of these components which can be expensive not only to buy but also to maintain. In addition, the VNA is extremely expensive and consequently limits low-cost and new applications of this concept.
iii) Time: in addition, placing the antennas precisely on the rail is time consuming and hence affects the speed of acquisition, which can be extremely long. For instance, the average time of one acquisition was in the order of several minutes, in some cases even up to 60.

For these reasons, a major update of the system has been conceived, planned, and developed, as described in Section IV.

III. MIMO Technique

In its conventional implementation, the MIMO technique requires each antenna element to transmit its own waveform. Orthogonality of the transmitted waveforms is a requirement for allowing separation at the receiver. However, it has to be clearly pointed out that, as the waveforms are to be applied to radar systems, the requirement of orthogonality (as intended in conventional communication systems), i.e.,

$$\int_0^T w_m(t) w_k^*(t) \quad dt = 0 \tag{1}$$

where $w_m(t)$ and $w_k(t)$ are two different waveforms limited between 0 and T, and * is the conjugate operator, is a necessary condition even if not sufficient. In fact, other properties, such as mutual low-cross-correlation, good Doppler tolerance, and good range resolution, are not only desirable, but mandatory, in order to ensure the correct operation of these systems so as

to outperform in some extent the conventional electronically steered array.

However, this is achievable at the cost of illuminating the entire space with an omnidirectional angle-dependent pattern [21]. If $w_k(t)$ is the generic transmitted band-limited pseudo-noise (PN) code, the overall transmitted waveform $w(t)$ at a distance R_0 (in the far field) and at an angle θ from the reference point can be expressed as

$$w(t,\theta) = \sum_{k=1}^{M} \frac{1}{R_k} w_k\left(t - \frac{R_0}{c}\right) \exp\left\{j2\pi\left(f_0 t - \frac{R_k}{\lambda}\right)\right\} \approx \frac{\exp\{j\phi\}}{R_0} \sum_{k=1}^{M} w_k\left(t - \frac{R_0}{c}\right) \exp\left\{j2\pi k \frac{d\sin\theta}{\lambda}\right\} \quad (2)$$

where M is the number of transmitters, d is the distance between two antennas in transmit, f_0 the carrier frequency, $\lambda = c/f_0$ the wavelength, and c is the speed of light

$$R_k = R_0 + kd\sin\theta \quad (3)$$

$$\phi = 2\pi\left(f_0 t - \frac{R_0}{\lambda}\right) \quad (4)$$

$$\frac{1}{R_k} \approx \frac{1}{R_0}. \quad (5)$$

As $w_k(t)$ is a pseudorandom sequence, also $w(t)$ is a PN code whose total power is the sum of the power of the single codes, as $w_k(t)$ is orthogonal to $w_m(t), \forall k \neq m$. The resulting waveform transmitted by a MIMO radar changes as a function of angle, as shown in (2) and [21], and it is possible to beamform passing the backscattered waveform $w(t)$ through N banks of M matched filters, which allow to distinguish the paths between each transmitter to each receiver.

The spacing in transmit and/or in receive between the elements is not required to be uniform. It can be actually demonstrated [11] that, being possible to distinguish the phases related to each single path between transmission and receive, e.g., using orthogonal PN codes, the combination of a N-element uniform linear array (ULA) spaced by $M\lambda/2$ in transmit (receive) and a M-element ULA spaced by $\lambda/2$ in receive (transmit) is equivalent to a ULA comprised by MN receivers spaced by $\lambda/2$, where one antenna only transmits an angle-dependent waveform with M-times the power of a single PN code. Additional and more sophisticated considerations on this topic can be found in [22] and are not reported here for brevity. Fig. 3(a) shows this concept through a sketch of a non-Nyquist-spaced transmit array (top), a Nyquist-spaced receive array (middle), and an equivalent array with only one transmitting element and MN Nyquist-spaced receiving elements.

When the echo from a (point) target is received [e.g., as in Fig. 3(b)], the phase history in the far field is shown in Table I (taking the central element as reference). It can be seen that the relative phase shift is a linear function of $d\sin\theta/\lambda$, where d is the spacing between two consecutive elements, and consequently this allows beamforming in receive as in a Nyquist-spaced arrays, in line with the equivalent model shown in Fig. 3(a). Hence, the benefit of this technique is in moving the beamforming to receive, after collecting the information

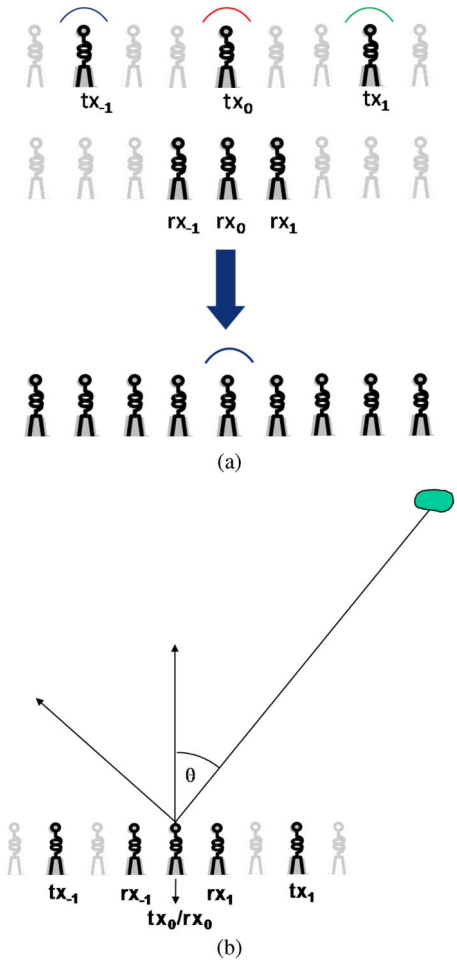

Fig. 3. Sketches of MIMO configurations. (a) MIMO transmit array (top), receive array (middle) and equivalent Nyquist-spaced array with one element only transmitting (bottom); (b) MIMO geometry for deriving equations as in Table I.

from all the angles at the same time, i.e., without scanning the beam. In addition, this technique allows to synthesize an array of MN elements with only $M+N$ physical elements. This allows for reduction of the complexity of the system, as it is required to control a reduced set of antennas only. However, these advantages are achievable at the cost of avoiding beamforming in transmission [21]. Consequently, it can be argued that, consequently, this technique suffers reduced Peak-to-SideLobes Ratio (PSLR), e.g., 13 dB against 26 dB for ULAs, but in fact, after an appropriate weighting on the receive array only, it can be demonstrated that this is a negligible issue.

If the same waveform is transmitted at the same time (or, alternatively, after processing appropriately the phases of the echoes of the PN codes after matched filtering), Fig. 4 shows the patterns generated by the arrays in Fig. 3(a), pointing at $\theta = 0$. As can be seen, the grating lobes in transmission[1] are compensated by the nulls in receive. In general, this is also true pointing at any angle. As a consequence, the MIMO radar technique can be considered as a development of minimum-redundancy linear arrays [23] through the introduction of codes at the element level.

[1]Due to the non-Nyquist spaced antennas.

TABLE I
MIMO PHASE SHIFTS FOR A GEOMETRY AS IN FIG. 3(b)

Tx Element	Rx Element	Absolute phase	Relative phase shift
tx_{-1}	rx_{-1}	$\exp\left\{-j2\pi\frac{R_0+4d\sin\theta}{\lambda}\right\}$	$-2\pi\frac{4d\sin\theta}{\lambda}$
tx_{-1}	rx_0	$\exp\left\{-j2\pi\frac{R_0+3d\sin\theta}{\lambda}\right\}$	$-2\pi\frac{3d\sin\theta}{\lambda}$
tx_{-1}	rx_1	$\exp\left\{-j2\pi\frac{R_0+2d\sin\theta}{\lambda}\right\}$	$-2\pi\frac{2d\sin\theta}{\lambda}$
tx_0	rx_{-1}	$\exp\left\{-j2\pi\frac{R_0+d\sin\theta}{\lambda}\right\}$	$-2\pi\frac{d\sin\theta}{\lambda}$
tx_0	rx_0	$\exp\left\{-j2\pi\frac{R_0}{\lambda}\right\}$	0
tx_0	rx_1	$\exp\left\{-j2\pi\frac{R_0-d\sin\theta}{\lambda}\right\}$	$2\pi\frac{d\sin\theta}{\lambda}$
tx_1	rx_{-1}	$\exp\left\{-j2\pi\frac{R_0-2d\sin\theta}{\lambda}\right\}$	$2\pi\frac{2d\sin\theta}{\lambda}$
tx_1	rx_0	$\exp\left\{-j2\pi\frac{R_0-3d\sin\theta}{\lambda}\right\}$	$2\pi\frac{3d\sin\theta}{\lambda}$
tx_1	rx_1	$\exp\left\{-j2\pi\frac{R_0-4d\sin\theta}{\lambda}\right\}$	$2\pi\frac{4d\sin\theta}{\lambda}$

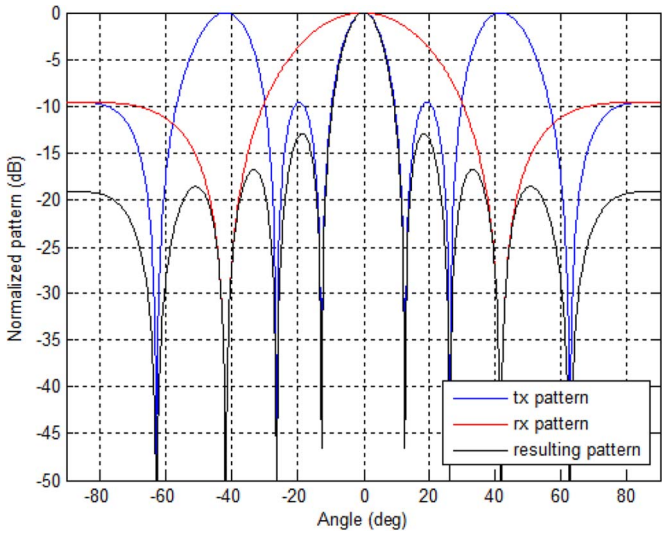

Fig. 4. Transmit, receive, and overall patterns for a MIMO array.

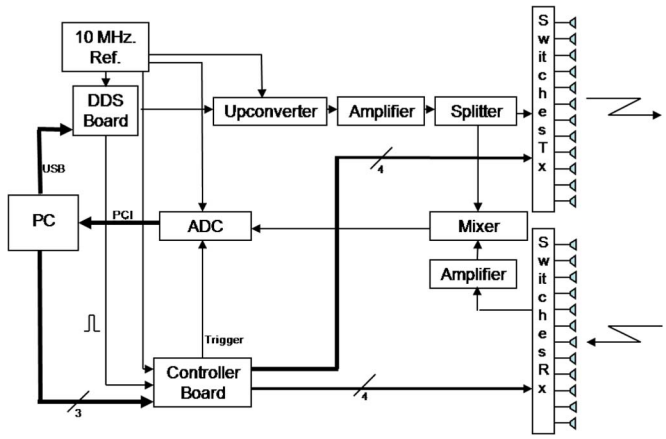

Fig. 5. MELISSA HW block design.

For the purposes of this paper, the most known PN or phase codes [17], [18] suffer poor Doppler tolerance, hence do not fit our requirements for the new system. In addition, using codes requires downconversion, Nyquist sampling and matched filtering, which are very likely to introduce tight constraints in HW design. Another requirement is the presence of as many matched filters (either hardware or software) as transmitted codes after each receiver, with a corresponding increase in costs and complexity of the overall system. Hence, the solution applied at this stage is to perform beamforming over a MIMO architecture through interleaved transmission and receive, as shown in the following section.

IV. MELISSA, THE JRC MIMO SYSTEM

The new JRC radar system, based on the MIMO technique, has been named MELISSA. Rather than moving the antennas sequentially on a rail, it has been decided to use a MIMO configuration, as just described. In line with the background of Section III, the effects of a non-Nyquist spaced transmission have been compensated by an appropriate antenna array in receive. In particular, it was decided to implement an FMCW radar [24] with switches on the tx and rx antennas in order to allow time-separation of the signals in receive. In other words, the tx and rx channels sequentially changes in time in order to measure the entire raw data matrix consisting of MN channels. This is obviously a tradeoff between the need of distinguishing the signals in receive and the current unavailability of robust PN codes.

For the purposes of this upgrade, it seems important to clearly highlight that having a transceiver sliding on a rail is exactly the same as building a MIMO array, as long as both their synthetic apertures are comprised of the same number of points spaced by the same distance.

A. MELISSA Overview

Fig. 5 shows a block diagram of the new system, which has been developed as follows.

MIMO Antenna Array: It was decided to use a MIMO array comprised of $M = 12$ antennas in transmission and $N = 12$ in receive. These numbers have been chosen because they are a good compromise for allowing a fair equivalent synthetic aperture while keeping the number of elements of the first implementation of this system relatively small. The antennas in transmission were set at $N(\lambda/2)$ from one another, while the receivers at $\lambda/2$. On the basis of availability, cost and performance, two kinds of antennas (horn and Vivaldi) fit our requirements. Horn antennas with approximately 13-dB gain and tailored for 11–18 GHz have been selected for transmission. These antennas are bigger than the transmitted wavelength, so they are generally not used in antenna arrays requiring a spacing at $\lambda/2$. However, because the MIMO technique allows antennas in transmission to be non-Nyquist spaced, horn antennas are one of the best tradeoffs because they have higher gain than dipoles and Vivaldi antennas and, at the same time, their pattern is still quite broad. On the receiver side, broadband (9–25 GHz) Vivaldi antennas have a gain of roughly 6 dB only and a pattern broader than the horns', but they can be easily spaced at $\lambda/2$.

FMCW Architecture and Switches: FMCW radars are mature, stable, and robust systems which also allow to reduce the complexity in receive. We refer to [24] for all the details. From a conceptual point of view, the technology used here is almost the same as LISA's, even if there are major differences in the way the signal is generated, as described later. As previously discussed, switches and antennas at preselected positions have been used in place of moving the positioner on the rail. As this is the first version of the major upgrade of LISA, the separation in time of the transmitted waveforms allowed also to keep the complexity of the system relatively low. Solid-state switches are known to have typical switching time which is much faster than that of the mechanical ones (≤ 1 μs versus $\approx$1 ms), even if they introduce an insertion loss (3–4 dB at best).

Controller, Waveform Generator, and Sampler: The system can be controlled through commercial PCs. The main task of the PC is to program the digital synthesizer which generates the FMCW and acquire data from the analog-to-digital converter (ADC). A standard chirp for FMCW using a low-cost, high-performance direct digital synthesizer (DDS) was chosen to generate the signal before the up-conversion. The DDS has an embedded fully programmable digital ramp generator (DRG). Its features include the possibility of setting the upper and lower frequencies, independent control of the step size, and rate for positive and negative slopes. Moreover, it can be easily controlled through a USB interface, has an embedded 14-bit digital-to-analog converter (DAC) and supports sample-rates up to 1 gigasamples per second with a maximum bandwidth of 400 MHz. In addition, it allows external synchronization through a reference clock (10 MHz). An interesting feature is that it also allows synchronization of multiple boards, which can be exploited in future developments of MELISSA. The results shown in this paper have been gathered using a saw-tooth ramp, being aware to synchronize the start of the switching time of the PIN Diode Switches. Finally, a 16-bit, two-channel digitizer with simultaneous sampling up to 20 MSPS megasamples per second has been used as an ADC. The digitizer has a deep memory option (up to 128 MS per channel) that allows flexibility in the way data can be acquired. The digitizer's configuration is determined by the user including sample rate, segmented memory, flexible trigger system, and data reduction feature for data transferred from memory.

Fig. 6. Test field.

In symbols, the ideal time-continuous signal $\hat{s}(t)$ generated by the cascade of DRG and DAC can be expressed as

$$\hat{s}(t) = \bar{V}_0 \cos\left(\pi \frac{B}{T} t^2\right) \mathrm{rect}_T(t) \tag{6}$$

where $\bar{V}_0$ is the amplitude of the signal as output from the DAC, B is its compressed bandwidth, T is its duration, and

$$\mathrm{rect}_T(t) = \begin{cases} 1, & 0 \leq t \leq T \\ 0, & \text{otherwise.} \end{cases} \tag{7}$$

After up-conversion and amplification, the signal fed to the switch in transmission can be expressed as

$$\tilde{s}(t) = A\hat{s}(t)\cos(2\pi f_0 t) \tag{8}$$

where f_0 is the carrier frequency and A is the gain of the amplifier before transmission, supposed ideal. Finally, in switching, the signal $s^m(t)$ transmitted by the mth antenna can be expressed as

$$s^m(t) = G_m \tilde{s}(t) \mathrm{rect}_{NT}\left(t - (m-1)NT\right) \tag{9}$$

where $m = 1 \ldots M$ and G_m takes into account the losses of the mth channel of the switch and the gain of the mth transmitting antenna. The overall switched transmitted signal, when scanning all the MN channels of the MIMO radar, can be therefore expressed mathematically as

$$s(t) = \sum_{m=1}^{M} s^m(t). \tag{10}$$

B. Antennas' Positions and Preliminary Simulations

To understand the correct positions of the antennas in the transmit and receive arrays, simulations have been made with the primary aim to identify an appropriate antenna geometry. In addition, simulated data provided a preliminary validation of the MIMO processing algorithms. They have also been employed to understand the possible origins of image artifacts. Fig. 6 shows a photograph of the test field, and Fig. 7 shows its plan and approximation as main point scatterers. In particular, there are five strong scatterers on the wall of the building on the left of the scenario and an additional one in the middle.

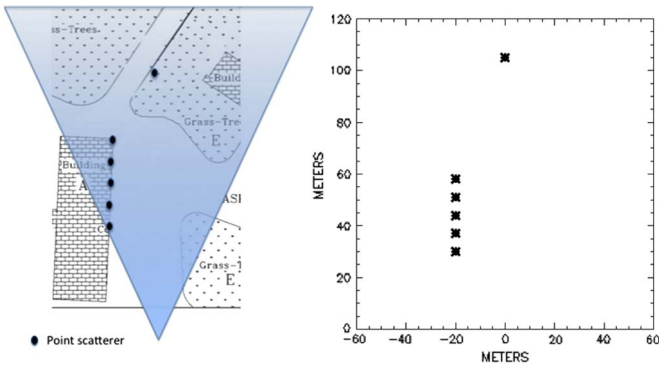

Fig. 7. (Left) Schematics of the test field and (right) its approximation for the simulations.

The latter is a metallic plate placed for calibration purposes. After the creation of the simulated raw data set, a conventional algorithm [8] has been employed to produce the image.

Assuming a Cartesian (x, y) plane with the transmitters and the receivers, respectively, located at

$$V_m^{tx} = \begin{pmatrix} x_m \\ y_m \end{pmatrix} \quad \text{and} \quad V_k^{rx} = \begin{pmatrix} x_k \\ y_k \end{pmatrix} \tag{11}$$

with $m = 1 \dots M$ and $k = 1 \dots N$, the targets have been placed at

$$V_h = \begin{pmatrix} x_h \\ y_h \end{pmatrix} \tag{12}$$

according to the positions of the scatterers in Fig. 7, with $h = 1 \dots 6$. The received signal $r_k^m(t)$ at the kth receiver from the mth transmitter has been modeled as

$$r_k^m(t) = \sum_h \left(\alpha_k^m[h] s^m \left(t - \frac{\rho_k^m[h]}{c} \right) \times \operatorname{rect}_T \left(t - (k-1)T \right) \right) + n(t) \tag{13}$$

where

$$\rho_k^m[h] = \left\| V_m^{tx} - V_h \right\| + \left\| V_k^{rx} - V_h \right\| \tag{14}$$

$\alpha_k^m[h]$ accounts for the amplification in receive and the parameters of the radar equation [25] on the $(k + mN)$th channel of the MIMO radar, including the phase shift due to propagation, and $n(t)$ groups all the possible nuisance. In the simulations, the latter term has been set to 0 and

$$\alpha_k^m[h] = \exp\left\{ j2\pi \frac{\rho_k^m[h]}{\lambda} \right\} \tag{15}$$

for simplicity. After beating and ADC (sampling at $t = qT_0$), the signal becomes

$$R_k^m[q] = \left[r_k^m(t) \otimes \tilde{s}(t) \right]_{t = qT_0} \tag{16}$$

where $\otimes$ is the correlation symbol, and T_0 is the sampling time of the ADC. The simulated image I shown in the following figures have been therefore realized focusing each point

$$V_0 = \begin{pmatrix} x_0 \\ y_0 \end{pmatrix} \tag{17}$$

on a rectangular grid as

$$I = I[x, y] = \sum_{k=1}^{N} \sum_{m=1}^{M} R_k^m \exp\left\{ -j2\pi \frac{\hat{\rho}_k^m}{\lambda} \right\} \tag{18}$$

where

$$\hat{\rho}_k^m = \left\| V_m^{tx} - V_0 \right\| + \left\| V_k^{rx} - V_0 \right\|. \tag{19}$$

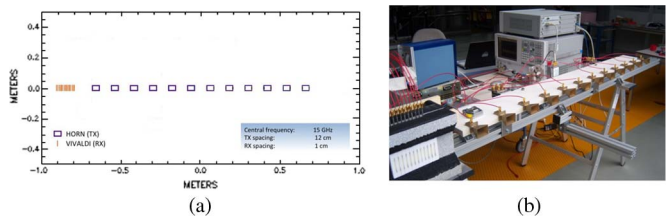

(a) (b)

Fig. 8. (a) Schematic and (b) photograph of MAG1 with the receiving array beside the transmitting.

There are faster and optimized methods for processing similar data sets [26], but at this stage, data processing was performed according to a robust method to validate the first results.

Two variants were considered in placing the transmit and receive array. Fig. 8(a) and (b) shows a schematic and a photograph, respectively, of the first placement of the antennas. As can be seen, in this first configuration (from now on called MAG1, i.e., MIMO Array Geometry 1), the receiving array is placed beside the transmitter. In this case, a relatively low coupling between transmission and receive has been observed in carrying out the experiments, because of the radiation patterns of the antennas.

The corresponding simulated image is shown in Fig. 10(a). Second-order effects, such as multi reflections have been ignored, and the scenario has been assumed bidimensional, for simplicity. A clear drawback of the geometry, is the presence of systematic replicas of the main lobe at specific positions. This can be explained by the fact that the gratings lobes in transmission are not perfectly compensated by the nulls in receive, since the receive array is slightly displaced to the side. This is also shown in Section IV-D with an analysis of some of the acquired data (Figs. 13 and 14). Nonetheless, this is a matter affecting the short range more than the far range, as the relative displacement of the arrays on far targets becomes negligible. Hence, the PSLR increases with distance, because the further the field, the smaller the relative displacement between tx and rx, and therefore the lower the replicas.

Fig. 9(a) and (b) shows, respectively, a schematic and a photograph of an alternative arrangement of the arrays, where the receivers are placed over the transmitters. We refer from now on to this configuration as MAG2, i.e., MIMO Array Geometry 2. Fig. 10(b) shows the simulated image in this case. If compared to Fig. 10(a), a reduction of the PSLR can be observed. However, taking into account the radiation pattern of the Vivaldi antennas, in actual experiments, the coupling

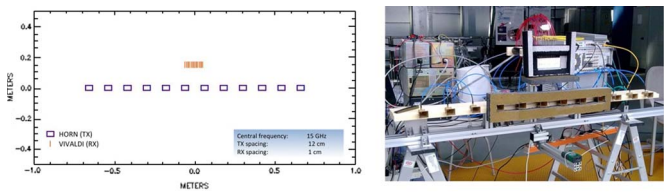

(a) (b)

Fig. 9. (a) Schematic and (b) photograph of MAG2 with the receiving array above the transmitting.

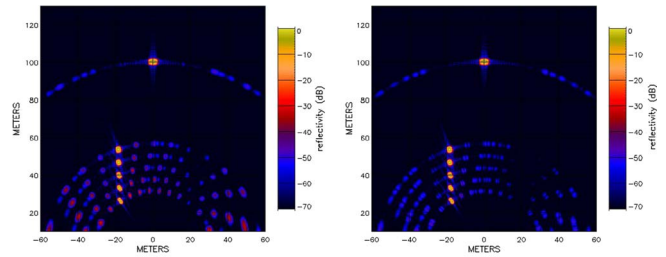

(a) (b)

Fig. 10. Simulated image of the schematic of the test field for (a) MAG1 and (b) MAG2.

between transmission and receive is expected to increase. It is worth noting that this configuration has a more efficient occupation of the space with respect to MAG1. The compactness of the system may become relevant in future developments where additional antennas will be deployed.

C. Choice of Parameters

In performing the experiments, the carrier frequency was set to 13.85 GHz, which is the maximum of the upconverter. As explained previously, M and N, i.e., the number of the antennas in tx and rx, respectively, were both set to 12. The ramp duration T of the FMCW signal, with a 100% duty cycle, was set according to the specification of maximum unambiguous range, i.e.,

$$R_u = \frac{cT}{2}. \tag{20}$$

Nevertheless, in FMCW radars, whenever the maximum sampling rate is $B_s \leq B$, (20) has to be modified [24] into

$$R_u = \frac{B_s}{B}\frac{cT}{2}. \tag{21}$$

In this case, B_s was set at 20 MHz, the maximum of the ADC.

Assuming a far target in a switched MIMO configuration as MELISSA's, it has to be noted that a moving target is be subject to a Doppler shift as $\exp\{j2\pi k f_d T\}$ across the MN synthesized channels, i.e., with $k = 0 \dots MN-1$, where

$$f_d = \frac{2v}{\lambda} \tag{22}$$

and v is the radial velocity of the target. Hence, in the same way as it occurs in conventional radars, an additional constraint on T is given by the not ambiguous Doppler, i.e.,

$$-\frac{1}{2T} \leq f_d < \frac{1}{2T}. \tag{23}$$

TABLE II
LISA—MELISSA COMPARISON AND EXPERIMENT PARAMETERS

	LISA	Experiments parameters	MELISSA final configuration
TX Elements (M)	1	12	16
RX elements (N)	1	12	16
Equivalent real aperture	≤ 3 m	1.44 m	2.56 m
Central frequency	11 to 17 GHz	13.85 GHz	13 to 15 GHz
Frequency band	≤ 400 MHz	180 MHz	≤ 400 MHz
Frequency step	any	375 kHz	any
Radiated power (CW)	≤ 30 dBm	26 dBm	≤ 33 dBm
Single ramp time T	0.5 sec	25μsec	any ($\geq 5\mu$s)
Time for a single full scan	1 to 60+ mins	3.6 msec	MN times T

In addition, $\exp\{j2\pi k f_d T\}$ is a function of the Doppler shift of the target and the time kT, $k = 1 \dots MN$, related to the kth channel. It is important to remark that the loss in coherency arising from these phase shifts may affect correct angle-focusing of moving targets in the same way as in conventional SAR systems. In more detail, a signal with a direction of arrival θ in the far field at the kth synthesized channel is subject to the following phase shift ϕ_k

$$\phi_k = 2\pi k\left(\frac{d}{\lambda}\sin\theta + f_d T\right) = 2\pi k\frac{d}{\lambda}(\sin\theta + \sin\epsilon_\theta) \tag{24}$$

where the substitution

$$\frac{d}{\lambda}\sin\epsilon_\theta = f_d T \tag{25}$$

i.e.,

$$\epsilon_\theta = \arcsin\left(\frac{\lambda}{d} f_d T\right) \tag{26}$$

has been made. Obviously, ϵ_θ is a measurement of the error in angle, due to the Doppler shift generated by the movement of the target throughout the switching. The Nyquist condition $d/\lambda = 1/2$ and that in (23) ensure that

$$-1 \leq \frac{\lambda}{d} f_d T < 1 \tag{27}$$

and consequently that ϵ_θ is real. In dimensioning the system, it was decided to accept a maximum error $|\epsilon_\theta| \leq 1^\circ$ at $v = 20$ km/h and to have a unambiguous range greater than 150 m, which is the approximate maximum distance of targets within the test field in Fig. 6. $T = 25$ μs and $B = 180$ MHz resulted in a good compromise for the constraint in (21), (23), and (24) for the purpose of demonstrating the concept of this paper. All the parameters are reported concisely in the central column of Table II. LISA's typical configuration and the parameters of the final version of MELISSA have been placed beside on the right and left, respectively, for comparison.

D. Calibration and Preliminary Results

Two different calibration procedures have been tested and compared: 1) a strong reflector of known characteristics (ideally a point scatterer—from now on referred as calibrator) placed in a known position and 2) an active transceiver also placed in a known position. Both procedures provided similar results. The calibrators have been placed as far as possible. This is because

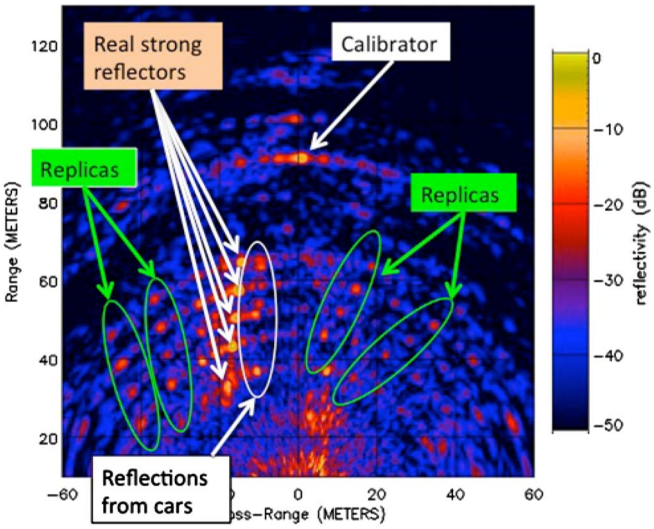

Fig. 11. Example of an image before calibration with replicas and other artifacts.

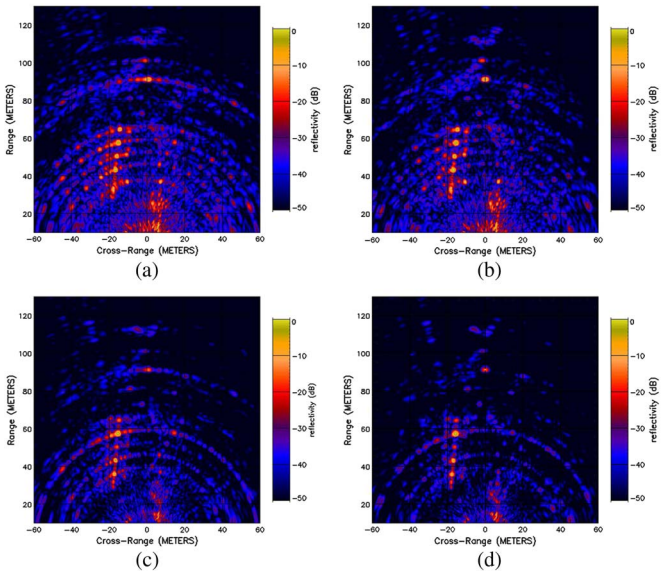

Fig. 12. Sensed environment, (up) MAG1 and (down) MAG2, (left) before and (right) after calibration. (a) MAG1, not calibrated system. (b) MAG1, calibrated system. (c) MAG2, not calibrated system. (d) MAG2, calibrated system.

using real objects for calibration requires a longer distance to minimize pointing effects. It is mandatory that all the antennas forming the MIMO are within the main beam of the calibrator.

Fig. 11 shows the obtained image of the test field in Fig. 6 using MELISSA in MAG1 without applying any calibration. The parameters of the acquisition are as in the central column of Table II. The main scatterers on the building on the left, as well as other targets, such as trees and vegetation on the right part and cars in front the building, are clearly visible. On the other hand, while sidelobes in range are negligible due to a Blackmann-Harris weighting function applied to the raw data, the image suffers very low PSLR in azimuth, and consequently it results noisy and unfit for practical applications.

Improvements in the quality of the obtained images are displayed in the sequence of images from Fig. 12(a)–(d). A first improvement in the PSLR has been achieved by calibrating the data acquired in MAG1 [Fig. 12(b)]. The images obtained before and after the calibration in MAG2 are displayed in Fig. 12(c) and (d), respectively. A reduction of the sidelobes can be observed, in line with the simulations of the previous section, when MAG2 is used instead of MAG1 [Fig. 12(a) versus Fig. 12(c); Fig. 12(b) versus Fig. 12(d)]. In particular, the last [Fig. 12(d)] shows that after calibration most of the artifacts have been removed, and the overall quality of the image has substantially improved.

This improvement resulting from the change of geometry can be explained analyzing the behavior of the calibrator in the center of the test field and recalling that the MIMO technique exploits the possibility of compensating the grating lobes in transmission with nulls in receive. This is analyzed in detail in Figs. 13 and 14, which show the position of the nulls in receive compared to the position of the first grating lobe in transmit, taking into account the echoes from the calibrator in Fig. 12(a) and (c) before calibration. Each of these figures is comprised of 24 plots, which are: 1) 12 plots gathered at each receiver when all the antennas transmit and 2) 12 plots gathered across all the receivers when the horn antennas transmit alternately. In both figures, the red and black thick lines indicate the average

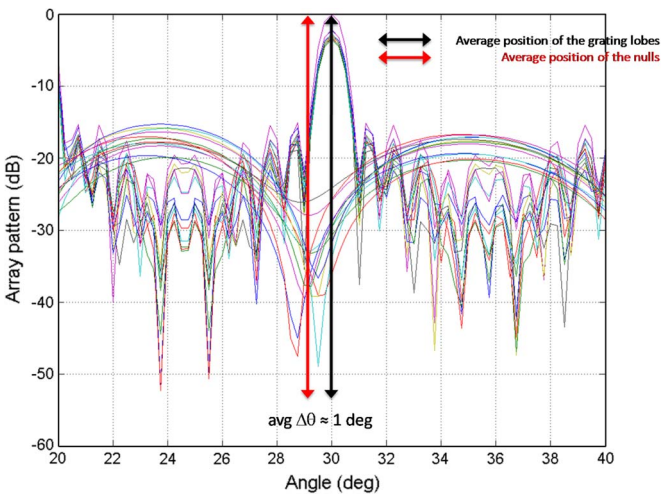

Fig. 13. First grating lobe and corresponding nulls, MAG1.

position of the nulls in receive and of the grating lobes in transmission, respectively. A noticeable reduction in mismatch of the position of nulls can be observed passing from MAG1 (approximately 1°) to MAG2 (approximately 0.3°), which in turn corresponds to a higher PSLR (lower replicas).

V. Moving Target Detection

In this section, we present some results of an additional and immediate application of MELISSA. These are to be intended as a demo of the new potential of this system and clearly do not provide a full outlook of the future applications. The main parameters of acquisition are reported in the central column of Table II with antennas positioned according to MAG2. In data processing, a simple and fast decluttering algorithm, i.e., a coherent background subtraction, has been applied to the images. In particular, after acquiring data when no moving targets are present, a difference between the acquired kth image

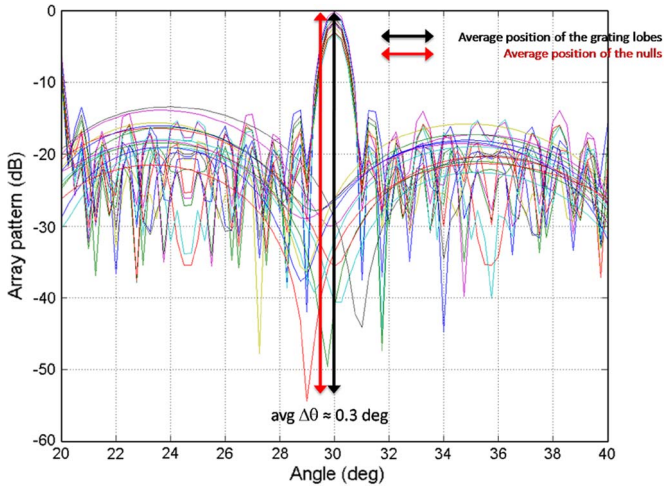

Fig. 14. First grating lobe and corresponding nulls, MAG2.

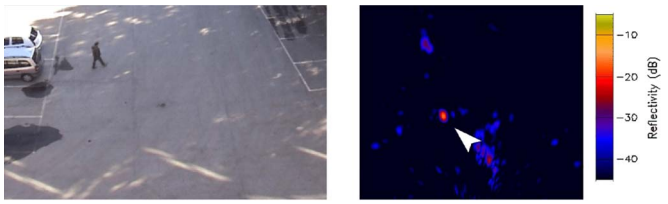

(a) (b)

Fig. 15. (a) Walking person and (b) differential image at the beginning of the acquisition.

I_k and a reference I_k^0 have been implemented. The differential image ΔI_k has been consequently produced as follows:

$$\Delta I_k = I_k - I_k^0 \tag{28}$$

where the reference I_0^k was updated as

$$I_k^0 = \frac{1}{H} \sum_{h=k-H}^{k-1} I_h \tag{29}$$

i.e., it was the average of $H = 30$ images previously acquired. Of course, there are more sophisticated and better ways to remove clutter, and we are aware that this easy technique works well with fixed clutter (i.e., cars, buildings, etc.) but not with vegetation, but, however, the aim is to provide a first insight into the performance of the upgraded system.

So far, the total time for a single acquisition (3.6 ms) is already short enough to assess on the possibility of detecting a "slow" moving target, such as a walking person. For this purpose, an experiment has been performed with a person walking in front of the system at a distance of about 30 m. Figs. 15(a) and 16(a) show two frames of the movie of the experiment and Figs. 15(b) and 16(b) the corresponding sensed results at the beginning and the end of the acquisition after removing fixed clutter.

In more general terms, the following can be remarked:

i) First of all, the moving target is generally well imaged at the correct position.

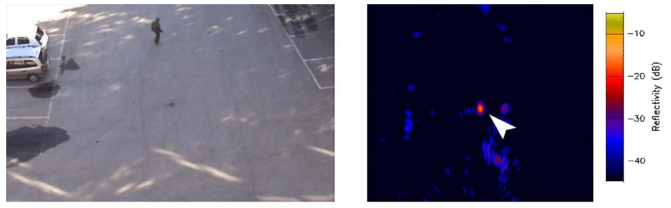

(a) (b)

Fig. 16. (a) Walking person and (b) differential image at the end of the acquisition.

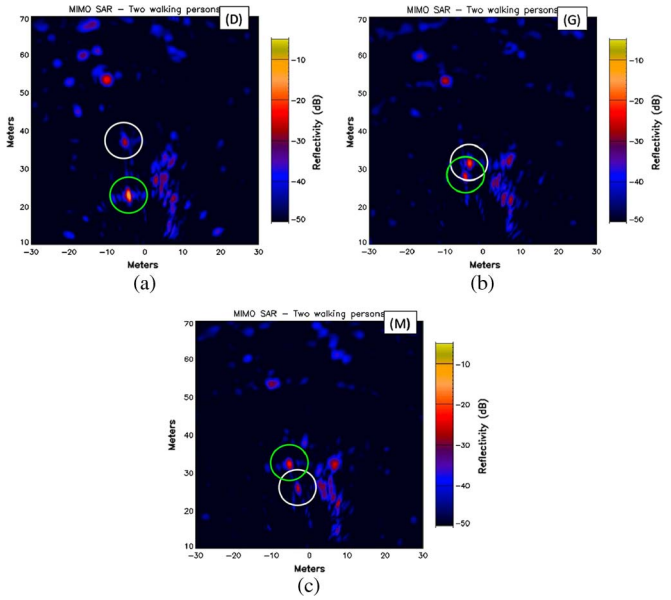

(a) (b) (c)

Fig. 17. Two walking targets at the beginning, middle, and end of the acquisition.

ii) The target seems to be focused correctly without defocusing, which may be expected if the acquisition time is not short enough.

iii) The target intensity is variable as it could be expected taking into account the nature of the target.

A second experiment was also performed with two people walking along a direction approximately perpendicular to the MIMO array. Fig. 17(a)–(c) shows the results at three different instants of time of the data acquisition. As can be seen, the high resolution allows to distinguish targets also when they are relatively close with one another.

VI. Discussion

In this paper, it has been shown that a MIMO system can match the performance of GB-SAR such as LISA. Nonetheless, while LISA is an optimized system and could improve its performance only through an increment of costs, the new system is cheaper, more agile, and more powerful and with an increased potential. In more detail, the following can be remarked:

i) Size of the synthetic aperture: in the shown prototype of MELISSA, the length of the MIMO synthetic aperture is approximately 1.44 m. Extending the array requires only additional antennas, while LISA requires a longer rail. Hence, from this point of view, MELISSA can have a number of arrays ready to be assembled one next to the

other in a scalable architecture, so to tailor the configuration to actual needs.

ii) Precision and cost: the precision issue has been moved through this upgrade from the positioner to manufacturing. Replacing the rail and the positioner with an appropriate number of low-cost antennas allows to remove most of the purchase and maintenance costs of the mechanical parts of LISA. Furthermore, replacing the VNA with a combination of a DDS for signal generation and a digitizer as ADC allowed additional savings.

iii) Time: as previously discussed, replacing a frequency-scan radar with a FMCW radar yield similar performance. These improvements led to a reduction of the acquisition time from minutes to milliseconds. Being independent of mechanical movements improves dramatically the speed of acquisition ($\leq$ 40 ms per image), so that the number of gatherable images is significantly increased. In turn the system's output, intended as number of images per second, is a function of the switching speed of the antennas and the speed of processing, not anymore of the mechanical movements of the positioner. It is therefore easy to understand that because of these changes the range of applications of MELISSA is wider than LISA's.

While traditional SAR systems, primarily for airborne and spaceborne applications, still remain an extremely valid and powerful tool, the proposed MIMO approach can represent a convenient alternative to conventional GB-SAR systems allowing a much higher acquisition rate. Nevertheless, Doppler-related issues have shown that parallelization in receive and, possibly, in transmit have to be pursued to lessen the constraints discussed in Section IV-C. In this sense, the full potential of these systems can be exploited only when robust PN codes are available. With regard to the physical dimension of the system, whenever the synthesized aperture increases, the advantages of MIMO tends to reduce because the number of antennas (as well as the complexity of the whole system) increases with a relevant impact on the cost.

VII. Conclusion and Future Work

In this paper, we described the update of an existing GB-SAR system (Section II) to a MIMO system (Section III), and we discussed the reasons for the upgrade, the preliminary studies, and the calibration issues (Section IV). We also provided some of the first results in literature obtained with a MIMO radar system (Section V) and some final considerations (Section VI). The overall work shown here had the main aim to implement a demonstrator of an innovative radar system able to improve significantly the performance of LISA, reducing its costs at the same time. Such a development has been conceived as the mandatory first step to enlarge the field of application of radar imaging techniques with special attention to emerging technologies applied to security.

The (long) acquisition time was definitely limiting LISA's potential. This depends on the chosen radar architecture (SF CW, based on a VNA) and on the use of a mechanical rail to realize the synthetic aperture. The MIMO radar concept, applied to time-interleaved transmission and receive, has been shown to be a smart solution for reducing the complexity and the cost of LISA, allowing at the same time to speed up the acquisition time. In addition, based on the innovative concept of MIMO, the synthetic aperture has been proved to be at least comparable with that generated by a mechanical scan. It is clear that the interleaved transmission is an emulation of the synthetic aperture, and therefore the difference between the two systems is actually subtle. Since the number of transmitters and receivers can be modified arbitrarily, it is possible to make the receiving array longer. In turn, this allows to separate the transmitting antennas further and consequently achieve an array length extremely hard to realize in practice. After simulations and proof-of-concept. the final prototype has been shown to include a number of cost-effective hardware solutions. Preliminary experiments have also been carried out to validate the implemented system.

LISA operates in "fixed" scenarios, where the target's position does not change more than a fraction of the wavelength during the acquisition, and it exhibits typical decorrelation artifacts for moving targets. Such an effect is due to noncoherency of the data. In other words, LISA, while performing optimally in staticscenarios, totally fails in detecting moving targets. Hence, in a more general and realistic situation, a system like MELISSA will not only minimize defocusing effects but can also correctly sense moving targets. This has been shown in Section V where it has been proved that it is now possible to correctly image walking people (5–8 km/h). Indeed, given the actual acquisition time, this result was expected and from additional preliminary considerations, it is possible to focus targets up to approximately 20 km/h, even if further experiments have not been yet performed.

As can be expected, future work will concern a number of aspects that can significantly improve the performance of MELISSA. Particular attention will be given to antenna elements, cables, and switches manufacturing. In addition the acquisition time can be reduced further by splitting the receiving part of the system in two parallel channels. Further parallelization is possible and is expected to have a limited impact on the costs. Obviously the ultimate aim is to exploit digital and possibly cheap solutions to utilize robust PN codes in transmission, as soon as they become available. Moreover, processing will be optimized to obtain real-time images, ideally at a rate of 25+ frames per second. The use of an acquisition card with onboard digital signal processing capabilities will be explored in this context. Finally, more sophisticated algorithms for clutter removal (when detecting moving targets) will be realized.

Acknowledgment

The authors gratefully acknowledge the helpful comments and suggestions of the reviewers of this manuscript.

References

[1] M. Maitre, *Processing of Synthetic Aperture Radar (SAR) Images*. Hoboken, NJ: Wiley, 2008.

[2] J. C. Curlander and R. N. McDonough, *Synthetic Aperture Radar: Systems and Signal Processing*. New York: Wiley, 1992.

[3] S. Claude, *Polarisation: Applications in Remote Sensing*. London, U.K.: Oxford Univ. Press, 2009.

[4] A. Hein, *Processing of SAR Data: Fundamentals, Signal Processing, Interferometry*. Berlin, Germany: Springer-Verlag, 2003.
[5] W. G. Carrara, R. S. Goodman, and R. M. Majewski, *Spotlight Synthetic Aperture Radar: Signal Processing Algorithms*. Norwood, MA: Artech House, 1995.
[6] A. Meta, P. Hoogeboom, and L. P. Ligthart, "Signal processing for FMCW SAR," *IEEE Trans. Geosci. Remote Sens.*, vol. 45, no. 11, pp. 3519–3532, Nov. 2007.
[7] G. De Grandi, E. Nezry, G. Kattenborn, and A. J. Sieber, "Experimental characterization of spatial statistics in polarimetric multifrequency airborne SAR data," vol. 2, pp. 807–812, Aug. 1993.
[8] J. Fortuny and A. J. Sieber, "Fast algorithm for near-field synthetic aperture radar processor," *IEEE Trans. Antennas Propag.*, vol. 42, no. 10, pp. 1458–1460, Oct. 1994.
[9] D. Leva, G. Nico, D. Tarchi, J. Fortuny-Guasch, and A. J. Sieber, "Temporal analysis of a landslide by means of a ground-based sar interferometer," *IEEE Trans. Geosci. Remote Sens.*, vol. 41, no. 4, pp. 745–752, Apr. 2003.
[10] A. Martinez-Vazquez and J. Fortuny-Guasch, "A GB-SAR processor for snow avalanche identification," *IEEE Trans. Geosci. Remote Sens.*, vol. 46, no. 11, pp. 3948–3956, Nov. 2008.
[11] D. Bliss, K. Forsythe, and G. Fawcett, "MIMO radar: Resolution, performance and waveforms," presented at the 14th Annu. Adaptive Sens. Array Process. Workshop, MIT, Jun. 6–7, 2006.
[12] J. Li and P. Stoica, *MIMO Radar Signal Processing*. New York: Wiley, 2008.
[13] P. F. Sammartino, C. J. Baker, and M. Rangaswamy, "Moving target localization with multistatic radar systems," in *Proc. IEEE Radarcon*, May 26–30, 2008, pp. 1–6.
[14] J. H. G. Ender and J. Klare, "System architectures and algorithms for radar imaging by MIMO-SAR," in *Proc. IEEE Radar Conf.*, May 2009, pp. 1–6.
[15] N. Gebert and G. Krieger, "Azimuth phase center adaptation on transmit for high-resolution wide-swath SAR imaging," *IEEE Geosci. Remote Sens. Lett.*, vol. 6, no. 4, pp. 782–786, Oct. 2009.
[16] J. Li, X. Zheng, and P. Stoica, "MIMO SAR imaging: Signal synthesis and receiver design," in *Proc. 2nd IEEE Int. Workshop CAMPSAP*, Dec. 2007, pp. 89–92.
[17] H. A. Khan and D. J. Edwards, "Doppler problems in orthogonal MIMO radars," in *Proc. IEEE Radar Conf.*, Apr. 24–27, 2006, pp. 244–247.
[18] H. Deng, "Polyphase code design for orthogonal netted radar systems," *IEEE Trans. Signal Process.*, vol. 52, no. 11, pp. 3126–3135, Nov. 2004.
[19] H. Rudolf and D. Tarchi, "Ku-Band front-end for LISA," European Comm., Joint Res. Center, Ispra, Italy, 1999, Tech. Rep.
[20] D. Tarchi, D. Leva, N. Casagli, R. Fanti, G. Luzi, M. Pieraccini, A. Pasuto, and S. Silvano, "Landslide monitoring by using ground-based SAR interferometry. An example of application to the Tessina landslide in Italy," *Eng. Geol.*, vol. 68, no. 1/2, pp. 15–30, Feb. 2003.
[21] P. F. Sammartino, C. J. Baker, and H. D. Griffiths, "Range-angle dependent waveform," in *Proc. IEEE Radar Conf.*, May 10–14, 2010, pp. 511–515.
[22] P. F. Sammartino, D. Tarchi, and C. J. Baker, "MIMO radar topology: A systematic approach to the placement of the antennas," in *Proc. 13th ICEAA*, Turin, Italy, Sep. 12–16, 2011, pp. 114–117.
[23] A. Moffet, "Minimum-redundancy linear arrays," *IEEE Trans. Antennas Propag.*, vol. AP-16, no. 2, pp. 172–175, Mar. 1968.
[24] I. V. Komarov and S. M. Smolskiy, *Fundamentals of Short-Range FM Radar*. Norwood, MA: Artech House, 2003.
[25] M. I. Skolnik, *Introduction to Radar Systems*. New York: McGraw-Hill, 1981.
[26] P. F. Sammartino, D. Tarchi, J. Fortuny-Guasch, F. Oliveri, and R. Giuliani, "Phase compensation and processing in MIMO radars," *Proc. IET Radar Sonar Navig.*, vol. 6, no. 4, pp. 222–232, Apr. 2012.

Dario Tarchi received the Laurea in physics from the University of Florence, Florence, Italy, in 1990.

In 1991, he joined the Nuclear Magnetic Resonance Laboratory, University of Florence, working on the implementation of models for nuclear magnetic resonance data analysis and interpretation. Since 1993, he has been with the Joint Research Centre, European Commission, Ispra, Italy, where he has been involved in the design, implementation, and operation of a portable linear synthetic aperture radar (SAR) system. His main research interests concern the application of SAR interferometric techniques for changes detection in natural and man-made objects and the development and testing of novel SAR systems for various applications.

Franco Oliveri received the Laurea in Ingegneria Elettronica (system design and control system design) summa cum laude from the University of Genoa, Genova, Italy, in 1983.

He started his professional experience working for one of the major European suppliers of military technology where he progressed from Design Engineer to become the Laboratory Manager of the C3I R&D Laboratory dealing with hardware and software design of military computers and communication systems. Subsequently, he worked as the R&D Director in Malaysia for a European major supplier of telecommunication systems in the area of narrowband equipment as well as fiber optics and the Global System for Mobile (GSM). His last working experience before joining the Joint Research Center was as Vice President Sales in charge of selling GSM-R and WiMAX equipment/systems. In 2006, he joined the Directorate General Joint Research Centre (JRC) of the European Commission where he worked on secure communication systems as well as on software-defined radio and cognitive radio systems. Then, he also worked on multiple input multiple output radar and common information sharing environment for the EU maritime domain.

Pier Francesco Sammartino received the Laurea in telecommunication engineering from the University of Rome "La Sapienza," Rome, Italy, in 2005, and the Ph.D. degree in electronic and electrical engineering from University College, London, U.K., in 2009.

Currently, he is a Postdoctoral Scientist with the Joint Research Center of the European Commission in the field of radar systems. Until May 2009, he was an Analyst in radar research with CEA Technologies in Canberra, Australia. His research interests include multiple-input multiple-output radars, digital beamforming, radar signal processing, electronically scanned and frequency diverse arrays, radar networks, interferometry, synthetic aperture radar imaging, and micro-Doppler techniques.